Force-dependent binding of vinculin to α-catenin regulates cell–cell contact stability and collective cell behavior

Rima Seddiki[a], Gautham Hari Narayana Sankara Narayana[a], Pierre-Olivier Strale[a,b], Hayri Emrah Balcioglu[b], Grégoire Peyret[a], Mingxi Yao[b], Anh Phuong Le[b,c], Chwee Teck Lim[b,c], Jie Yan[b], Benoit Ladoux[a,b], and René Marc Mège[a,*]

[a]Institut Jacques Monod, Centre National de la Recherche Scientifique, CNRS UMR 7592, Université Paris-Diderot, 75205 Paris Cedex 13, France; [b]Mechanobiology Institute, National University of Singapore, Singapore 117411; [c]Department of Biomedical Engineering, National University of Singapore, Singapore 117542

ABSTRACT **The shaping of a multicellular body and repair of adult tissues require fine-tuning of cell adhesion, cell mechanics, and intercellular transmission of mechanical load. Adherens junctions (AJs) are the major intercellular junctions by which cells sense and exert mechanical force on each other. However, how AJs adapt to mechanical stress and how this adaptation contributes to cell–cell cohesion and eventually to tissue-scale dynamics and mechanics remains largely unknown. Here, by analyzing the tension-dependent recruitment of vinculin, α-catenin, and F-actin as a function of stiffness, as well as the dynamics of GFP-tagged wild-type and mutated α-catenins, altered for their binding capability to vinculin, we demonstrate that the force-dependent binding of vinculin stabilizes α-catenin and is responsible for AJ adaptation to force. Challenging cadherin complexes mechanical coupling with magnetic tweezers, and cell–cell cohesion during collective cell movements, further highlight that tension-dependent adaptation of AJs regulates cell–cell contact dynamics and coordinated collective cell migration. Altogether, these data demonstrate that the force-dependent α-catenin/vinculin interaction, manipulated here by mutagenesis and mechanical control, is a core regulator of AJ mechanics and long-range cell–cell interactions.**

Monitoring Editor
Manuel Théry
CEA, Hopital Saint Louis

Received: Apr 11, 2017
Revised: Nov 20, 2017
Accepted: Dec 14, 2017

INTRODUCTION

Adherens junctions (AJs) contribute both to tissue stability and dynamic cell movements. The cadherin–catenin adhesion complex is the key component of an AJ that bridges neighboring cells and the actin–myosin cytoskeleton, and thereby contributes to mechanical coupling between cells, which drives both cell assembly stability and dynamic cell movements during morphogenetic and tissue repair events (Guillot and Lecuit, 2013; Takeichi, 2014; Collins and Nelson, 2015; Mayor and Etienne-Manneville, 2016). Central to this process is the dynamic link of the complex to actin filaments (F-actin; Mege and Ishiyama, 2017). Cadherin cytoplasmic tail binds to β-catenin, which in turn binds to the F-actin binding protein α-catenin. α-Catenin then links cadherin–β-catenin adhesion complexes to the force-generating actomyosin networks, directly and/or indirectly through other actin binding proteins such as vinculin or afadin.

In addition, mechanotransduction at AJs enables cells to sense, signal, and respond to physical changes in their environment, and the cadherin–catenin complex has emerged as the main route of propagation and sensing of forces within epithelial and nonepithelial tissues (Leckband and Prakasam, 2006; Huveneers and de Rooij, 2013; Hoffman and Yap, 2015; Ladoux *et al.*, 2015). A proposed mechanotransduction pathway involves the myosin II–generated force-dependent change of conformation of α-catenin regulating

This article was published online ahead of print in MBoC in Press (http://www.molbiolcell.org/cgi/doi/10.1091/mbc.E17-04-0231) on December 27, 2017.

*Address correspondence to: René Marc Mège (rene-marc.mege@ijm.fr).

Abbreviations used: AJ, adherens junction; AOTF, acousto-optic tunable filter; ECM, extracellular matrix; FN, fibronectin; FRAP, fluorescence recovery after photobleaching; GFP, green fluorescent protein; HEPES, 4-(2-hydroxyethyl)-1-piperazineethanesulfonic acid; KD, knocked down; MDCK, Madin–Darby canine kidney; MI, modulation domain I; MII, modulation domain II; MIII, modulation domain III; NHS, *N*-hydroxysuccinimide; PAA, polyacrylamide; PBS, phosphate buffer saline; PDMS, polydimethylsiloxane; PIV, particle imaging velocimetry; ROI, region of interest; TEMED, tetramethylethylenediamine.

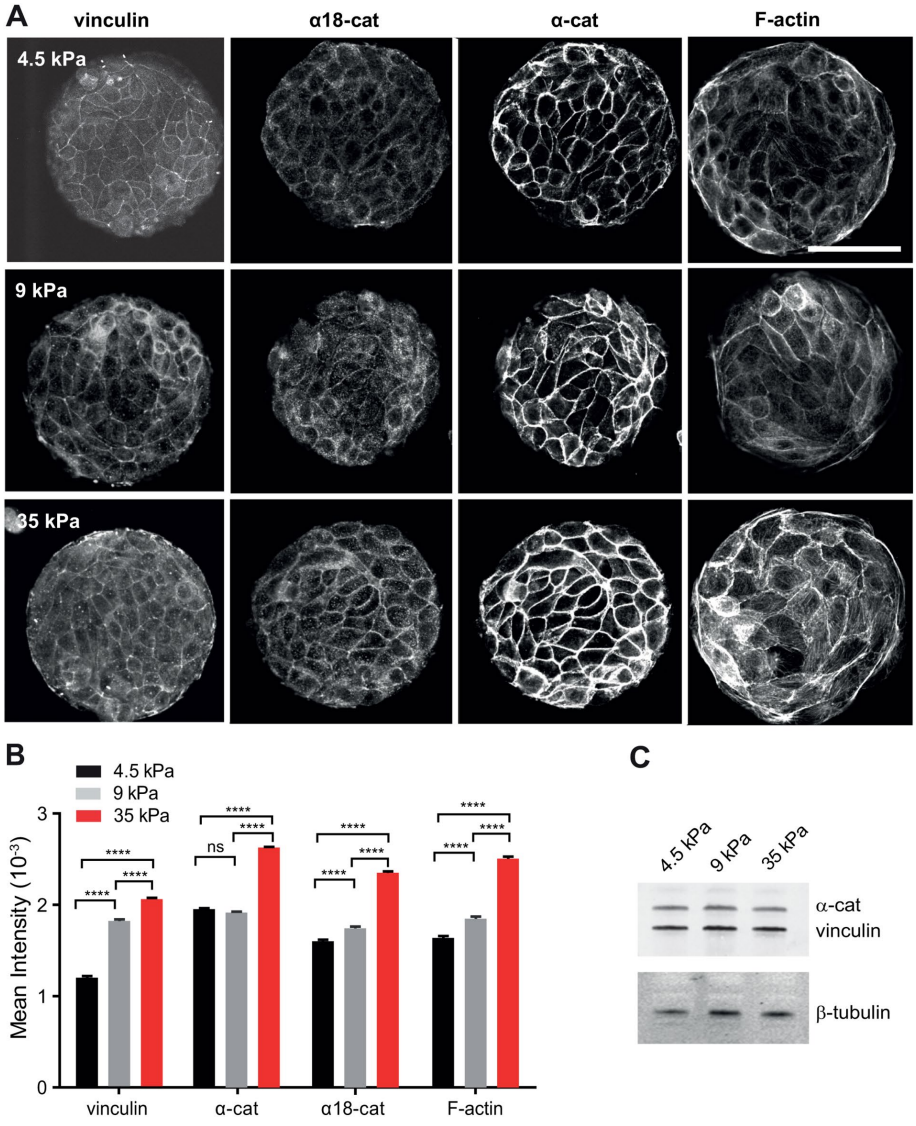

FIGURE 1: Substrate stiffness-dependent recruitment of α-catenin, vinculin and F-actin at cell–cell contacts. (A) MDCK cells were cultured for 24 h on PAA gels of the indicated stiffness (4.5, 9, or 35 kPa), on which 100-μm-diameter disks of FN had been patterned. Preparations were then fixed and immunostained for α-catenin, α18 epitope, vinculin, and F-actin and then imaged by confocal microscopy (panels show 0.5-μm-thick z-projections taken at the level of the apical complexes). Scale bar: 50 μm. (B) The histograms represent the mean fluorescence intensities measured for αE-catenin, α18 epitope, vinculin, and F-actin stainings as indicated in *Materials and Methods* (mean ± SEM, $n = 640–1260$ junctions in total per condition, out of three independent experiments; ****, $p < 0.0001$; ns, not significant; one-way analysis of variance (ANOVA) test. (C) Western blot analysis of α-catenin and vinculin from protein extracts of cells grown for 24 h on FN-coated PAA gels of 4.5, 9, and 35 kPa rigidity, respectively. α-Tubulin was used as a loading control.

vinculin recruitment (le Duc *et al.*, 2010; Yonemura *et al.*, 2010; Thomas *et al.*, 2013). At the single molecule force level, it has been shown that α-catenin reversibly unfolds upon forces in the range of those developed by a few myosin motors, allowing the binding of vinculin head (Yao *et al.*, 2014; Maki *et al.*, 2016). The tension-dependent binding of vinculin to α-catenin may thus be central to the adaptation of cadherin-dependent cell–cell contacts experiencing tugging forces in dynamic epithelial layers (Kim *et al.*, 2015; Han *et al.*, 2016; Jurado *et al.*, 2016), and may contribute directly to tissue mechanics and collective cell behavior. However, how this molecular pathway contributes to the dynamics of cell–cell contacts, and allows cells to locally sense, transduce, and adapt to environmental mechanical constraint is not well understood.

Here, we tackled this question by investigating the contribution of the force-regulated interaction between vinculin and α-catenin to AJ dynamics and collective cellular behavior. Indeed, it has been difficult to address this question so far, at least in mammalian cells, because in addition to the pleiotropic effect of α-catenin loss of function described in vivo (Torres *et al.*, 1997; Vasioukhin *et al.*, 2001; Lien *et al.*, 2006; Silvis *et al.*, 2011), the knock out of the protein in cells in vitro leads to the complete inhibition of cadherin-mediated adhesion (Vermeulen *et al.*, 1995; Benjamin *et al.*, 2010; Thomas *et al.*, 2013), as well as to cadherin-independent alteration of actin dynamics, subsequently affecting cell interaction with the extracellular matrix (ECM) (Benjamin *et al.*, 2010; Hansen *et al.*, 2013). To address the role of the tension-dependent association of α-catenin and vinculin, we generated mutant α-catenin proteins either unable to bind vinculin or constitutively bound to vinculin, and analyzed their effect on cell–cell contact stability and collective cell behavior when expressed in α-catenin–depleted epithelial cells.

RESULTS AND DISCUSSION

α-Catenin, vinculin, and F-actin recruitment at cell–cell contacts is dependent on intercellular stress in epithelial monolayers

Previous data have shown that vinculin recruitment at cell–cell contacts was dependent on tension. However, these data were obtained either by inhibiting intracellular contractility (le Duc *et al.*, 2010; Yonemura *et al.*, 2010) or by applying external forces (le Duc *et al.*, 2010; Dufour *et al.*, 2013). To directly determine the impact of intercellular stress physiologically generated by cell-borne contractile forces, we plated Madin-Darby canine kidney (MDCK) cells on fibronectin (FN)-patterned polyacrylamide gels of controlled stiffnesses of 4.5, 9, and 35 kPa and looked at the impact on the recruitment of vinculin, α-catenin, and F-actin. The junctional recruitment of these three proteins significantly increased with substrate stiffness (Figure 1, A and B). This enrichment did not result from increased cellular protein levels as shown by Western blot (Figure 1C). Moreover, we did not detect significant changes in junctional accumulation of E-cadherin as a function of substrate stiffnesses (1.36 ± 0.12, 1.30 ± 0.11, and 1.33 ± 0.04 A.U. for substrate stiffnesses of 4.5, 9, and 35 kPa, respectively), indicating that there was indeed a specific enrichment in α-catenin, vinculin, and F-actin at constant density of junctional E-cadherin. Thus, the junctional recruitments of α-catenin, vinculin, and F-actin are positively controlled by the intercellular tension

imposed by the matrix stiffness. The staining at cell–cell contacts with an antibody recognizing α-catenin under its open conformation also increased with substratum rigidity, suggesting a central contribution of the tension-dependent conformational change of α-catenin and recruitment of vinculin to the physiological adaptation to the force of AJs.

Vinculin binding to α-catenin is not required for the formation of cell–cell junctions but stabilizes junctional α-catenin

To address the role of the α-catenin/vinculin interaction in the tension-dependent regulation of cell–cell contacts, we generated α-catenin mutants unable to bind vinculin (α-cat-L344P) or binding constitutively to vinculin (α-cat-Δmod), respectively (Figure 2A). Vinculin binds to α-catenin within modulation domain I (MI), and substitution of lysine 344 by proline has been reported to impair vinculin binding (Peng *et al.*, 2012; Yao *et al.*, 2014). Modulation domains II (MII) and III (MIII) (residues 509–628) are autoinhibitory domains interacting with the MI domain and masking the accessibility of the vinculin-binding domain (Desai *et al.*, 2013; Maki *et al.*, 2016). This autoinhibition is released upon force-dependent stretching, unmasking the vinculin-binding domain (Yao *et al.*, 2014). Deletion of residues 509–628 (Δmod mutation) thus generates an α-catenin isoform constitutively binding to vinculin.

We analyzed the consequences of the expression of these variants on cell–cell contact restoration in α-catenin–depleted MDCK cells that do not form AJs (Benjamin *et al.*, 2010). The expression of α-cat-L344P and α-cat-Δmod restored the formation of cell–cell contacts that were indistinguishable from those of wild-type α-catenin–expressing cells (α-cat-wt; Figure 2B). The recruitment of vinculin at intercellular junctions in α-cat-Δmod–expressing cells (1.04 ± 0.02, n = 20) was significantly higher compared with α-cat-wt–expressing cells (0.67 ± 0.01, n = 31, p value < 0.0001), and significantly lower in α-cat-L344P–expressing cells (0.34 ± 0.06, n = 24, p value < 0.0001, one-way ANOVA test), whereas the recruitment of vinculin at the cell–substratum interface was comparable for the three cell types (Supplemental Figure S1). Thus, the two forms of α-catenin allow the formation of AJs in confluent MDCK monolayers, despite their impaired interaction with vinculin. The residual accumulation of vinculin at cell–cell contacts in α-cat-L344P cells may result from the interaction of vinculin with β-catenin reported previously (Peng *et al.*, 2010; Ray *et al.*, 2013). However, we also measured an ~30% residual vinculin staining at cell–cell contacts of α-cat-wt–expressing cells after 2 h of blebbistatin treatment (Supplemental Figure S2). Thus, the incomplete disappearance of junctional vinculin signal both in blebbistatin-treated α-cat-wt and in α-cat-L344P–expressing cells may merely be explained by the local contribution of cytoplasmic vinculin staining. In contrast, blebbistatin treatment had no significant effect on the accumulation of vinculin at cell–cell contacts of α-cat-Δmod–expressing cells (Supplemental Figure S2), validating the effect of the Δmod mutation on tension-dependent vinculin binding.

To assess the effect of the alteration of the tension-dependent binding of vinculin to α-catenin on the stability of AJs, we performed fluorescence recovery after photobleaching (FRAP) experiments on GFP-α-catenin at cell–cell contacts. The fluorescence recovery was similar for wt and Δmod α-catenin with ~50% of the molecules in the fast recovering, diffusion-limited fraction (Figure 2, C and D). However, the fluorescence recovery for the L344P mutant was significantly increased with a mobile fraction of α-catenin that was doubled (Figure 2, C and D) without changes in half recovery time (Supplemental Figure S2A). Interestingly, E-cadherin stability at cell–cell contacts was barely dependent on the binding of α-catenin to vinculin (Supplemental Figure S3, A and B). α-Catenin is, however, a complex molecule (Kobielak and Fuchs, 2004) and mutations

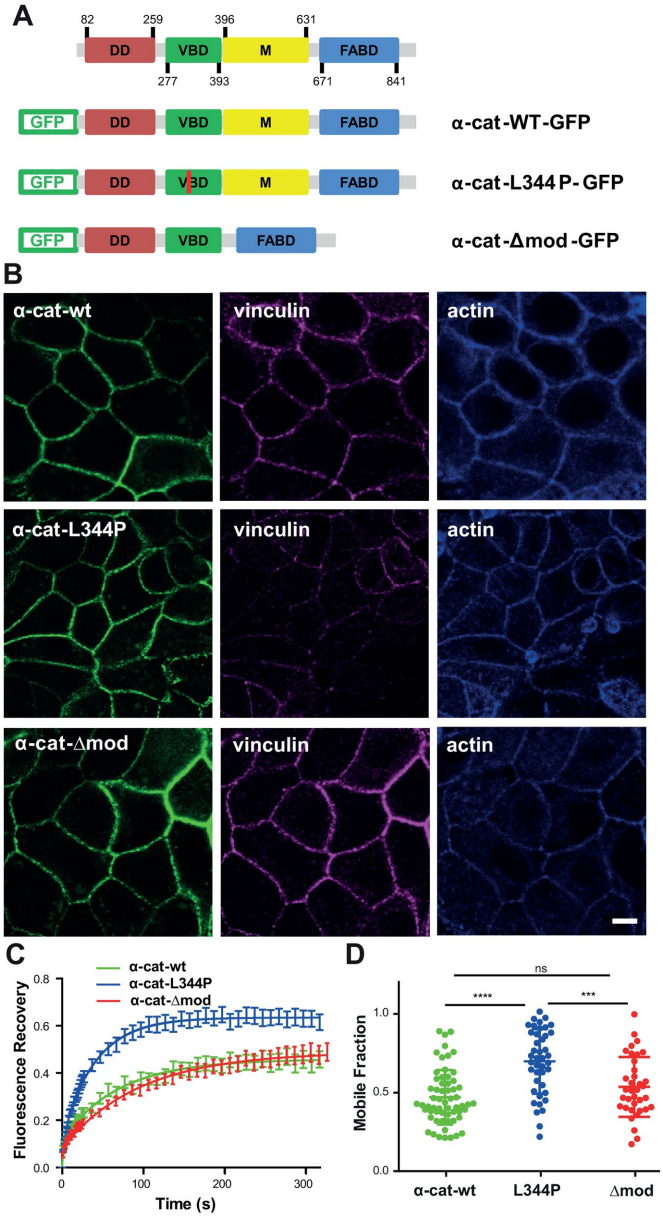

FIGURE 2: E-cadherin–dependent cell–cell contacts form independently of α-catenin/vinculin interactions. (A) Schematics of GFP-tagged wild-type (α-cat-wt-GFP), L344P (α-cat-L334P-GFP), and Δmod (α-cat-Δmod-GFP) αE-catenin constructs. (B) Confocal analysis of apical vinculin and F-actin distribution in αE-catenin KD MDCK cells expressing α-cat-wt, α-cat-L334P, and α-cat-Δmod grown on glass surfaces. The expression of mutant proteins restored cell–cell contacts, as did the expression of wt α-catenin. Scale bar: 5 μm. (C) FRAP experiments were performed on cell–cell contacts of α-cat-wt (green), α-cat-L334P (blue), or α-cat-Δmod (red)-expressing cells grown on glass substrates. Mean intensity recoveries over time (±SEM) fitted with a one-term exponential equation (n = 50 regions of interest out of three independent experiments for each condition). (D) Mobile fractions extracted from the fits of individual recovery curves (scatter dot plot, mean values ± SD). ****, p < 0.0001; ***, p < 0.001; ns, nonsignificant; one-way ANOVA test.

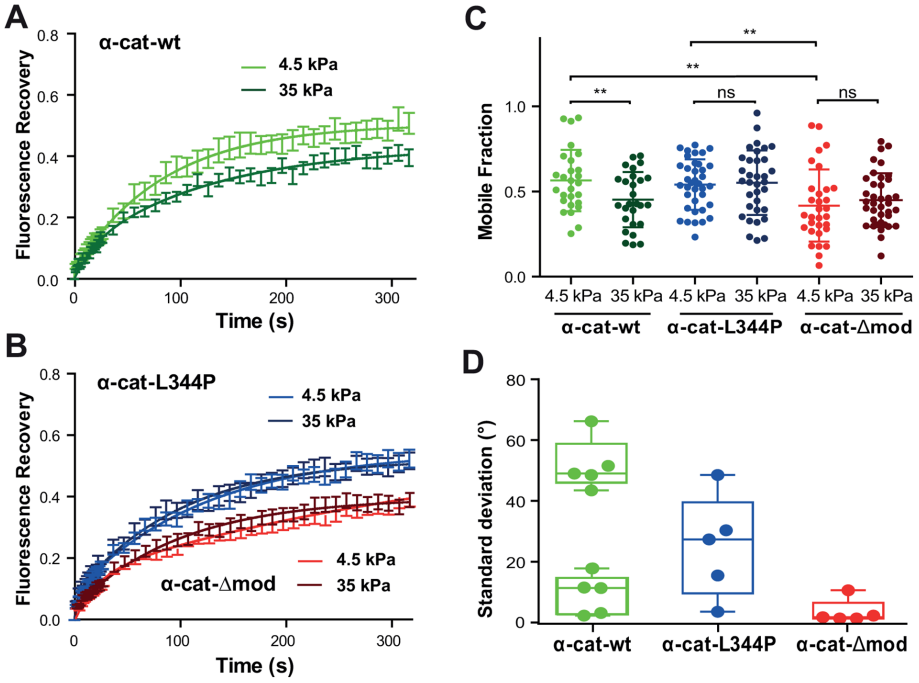

FIGURE 3: Binding of α-catenin to vinculin is required for its tension-dependent stabilization at cell–cell contacts. (A, B) MDCK α-catenin–KD cells expressing GFP-tagged α-cat-wt (green), α-cat-L334P (blue), or α-cat-Δmod (red) were cultured for 24 h on 4.5 (light colors) or 35 kPa (dark colors) PPA gels before FRAP experiments were performed. Graphs represent mean GFP fluorescence recovery over time (±SEM, $n = 50$ out of three independent experiments for each condition) fitted with a one-term exponential equation. (C) Mobile fraction values (scatter dot plot, mean values ± SD) extracted from the fits of individual recovery curves considered in panels A and B. **, $p < 0.01$; ns, nonsignificant; two-way ANOVA test. Notice the nonsignificant differences in mobile fraction values observed for the mutant proteins on soft and stiff substrates, contrasting with the significant decrease in mobile fraction observed for the wt protein as a function of increasing substrate compliance. (D) Magnetocytometry applied on Ecad-Fc–coated bead doublets bound to the surface of MDCK cells expressing α-cat-wt, α-cat-L334P, and α-cat-Δmod mutants. The histogram reports the mean values of the SD of the bead fluctuation angles.

analyzed here may have perturbed binding sites for others partners. Thus, to exclude this hypothesis we analyzed the mobility of α-cat-wt (fused to mCherry) in MDCK vinculin knockdown cells (Sumida *et al.*, 2011). We found that α-cat was also strongly destabilized in these conditions with a mobile fraction of 0.72 ± 0.06. Thus, vinculin binding to α-catenin is dispensable for the formation of intercellular contacts per se, but is required for the stabilization of junctional α-catenin in confluent monolayers. Vinculin binding may stabilize α-catenin by preventing its refolding following its force-dependent unfolding (Yao *et al.*, 2014). This may—via a force-dependent global conformational switch of α-catenin—shift α-catenin and the cadherin–catenin complex into a strongly F-actin bound state, thereby creating a self-reinforcing system for strong linkage of the complex to the actin cytoskeleton (Buckley *et al.*, 2014; Ladoux *et al.*, 2015). Vinculin may also stabilize α-catenin at AJs by providing additional binding interfaces between cadherin complexes and F-actin, thanks to the F-actin binding domain of vinculin (Yonemura *et al.*, 2010; Thomas *et al.*, 2013). Previous studies indeed indicate that the anchoring of cadherin complexes to F-actin by the actin binding site of vinculin in the absence of α-catenin actin binding domain is sufficient to restore E-cadherin–dependent cell contacts (Thomas *et al.*, 2013; Chen *et al.*, 2015; Jurado *et al.*, 2016) and that these junctions are even more stable than wt AJs (Chen *et al.*, 2015). Vinculin incorporation in the cadherin–catenin adhesion complex may thus increase its stability. Whatever is the exact molecular mechanism, vinculin binding under the control of a tension-dependent conformational switch of α-catenin may explain the observed substrate rigidity-dependent stabilization of α-catenin, vinculin, and F-actin at AJs.

Binding of vinculin is required for the tension-dependent stabilization of α-catenin at cell–cell contacts

To further determine the requirement of the α-catenin/vinculin interaction in the tension-dependent adaptation of cell–cell contacts, we analyzed the dynamics of junctional α-cat-wt, α-cat-L344P, and α-cat-Δmod in cells seeded on polyacrylamide (PAA) substrates of 4.5 or 35 kPa stiffness (Figure 3). FRAP experiments performed on α-cat-wt–expressing cells revealed a significant stiffness-dependent change in junctional α-catenin dynamics, with a higher mobile fraction on the more compliant substrate (Figure 3, A and C). In contrast, the dynamics of the α-catenin mutants were independent of substrate stiffness (Figure 3, B and C). The mobile fraction of α-cat-L344P was similar on both substrates and comparable to the mobile fraction value observed for the wt α-catenin on soft substrate. The mobile fraction of junctional α-cat-Δmod was also independent of the substratum compliance, but was significantly lower and comparable to the value obtained for wt α-catenin on stiff substrate. The characteristic recovery half times were not significantly different among these different conditions (Supplemental Figure S2B). The dynamics of E-cadherin did not change significantly with substrate compliance, or with α-catenin mutations (Supplemental Figure S3), in agreement with the observed vinculin-independent recruitment of E-cadherin around cell-bound E-cadherin–coated beads (le Duc *et al.*, 2010). These data show that the molecular stability of α-catenin at AJs is mechanosensitive, and that this mechanosensitive stabilization requires the binding to vinculin. Altogether, they suggest that the tension-dependent binding of vinculin to α-catenin regulates the stiffness-dependent stabilization of cadherin adhesion complexes at cell–cell contacts.

Vinculin/α-catenin association controls E-cadherin coupling to cortical actin

To test whether vinculin binding controls the mechanical coupling of cadherin complexes to the underlying actin cytoskeleton, we performed magnetocytometry experiments using superparamagnetic Ecad-Fc–coated beads bound on α-cat-wt–, α-cat-L344P–, and α-cat-Δmod–expressing cells. Torque was applied to bound beads by rotating a pair of permanent magnets 360° in both clockwise and counterclockwise directions, and the SD of fluctuation angles of the beads was obtained to quantify the response to the applied torque (Figure 3D). This measurement can be considered as a proxy of the stiffness of the mechanical link between cadherins and the cell cortex (le Duc *et al.*, 2010). For cells expressing

α-cat-wt, bead fluctuation angles showed two populations: half the beads loosely attached (mean SD = 51.8 ± 3.8°) and the other half strongly coupled (mean SD = 9.2 ± 2.9°). Thus, E-cadherin beads bound to wt α-catenin–expressing cells were either tightly or loosely coupled to the cortical cytoskeleton, indicating a complex regulation of the linkage between cadherin complexes and the cell cortex. Whether the two states were associated to differences in the lifetime of the bead–cell contact or to specific sites of binding of the bead on the cell surface are questions that could not be addressed with the present approach. In contrast, the mean SD of the bead fluctuation angle was centered to 25.1 ± 7.5° for cells expressing α-cat-L344P, indicating a very loose coupling to the cell cortex. In contrast, the mean SD was close to 0 (3.5 ± 1.8°) for cells expressing α-cat-Δmod, indicating a very stiff link of cadherins to the cortical actin (Figure 3D). These results demonstrate that the binding of α-catenin to vinculin is required for efficient mechanical coupling of cadherin–catenin complexes to the underlying cortical cytoskeleton. Altogether, our findings suggest that the mechanosensitive α-catenin/vinculin interaction, by contributing to tension-dependent cell–cell contact stability, regulates tissue mechanics.

Vinculin/α-catenin association controls collective cell dynamics

Although the role of α-catenin in epithelial tissue mechanics and collective cell behavior is well established (Vedula *et al.*, 2012; Doxzen *et al.*, 2013; Bazellieres *et al.*, 2015), the contribution of the tension-dependent association of vinculin to α-catenin remains unknown. To address the specific role of the binding of vinculin to α-catenin in epithelial tissue mechanics, we analyzed and compared the dynamics of confluent monolayers of mutant expressing cells, α-cat-wt–expressing cells, and parental α-cat knocked down (KD) cell monolayers, seeded on 500 μm Ø circular patterns coated with FN (Figure 4A and Supplemental Videos 1–4). α-cat-Δmod and α-cat-wt cells displayed slow and coordinated movements. In contrast, α-cat KD and α-cat-L344P cells behave as mesenchymal-like cells, displaying more rapid and uncoordinated motions as described previously for α-cat KD cells (Vedula *et al.*, 2012). The heat map of velocity fields obtained by particle imaging velocimetry (PIV) analysis further revealed higher velocities for α-cat KD and α-cat-L344P cells than for α-cat-Δmod and α-cat-wt cells (Figure 4B). The average velocities were the highest for α-cat KD cells, then significantly decreased for α-cat-L344P cells, and finally for α-cat-wt and α-cat-Δmod cells (Figure 4C). The spatial velocity correlation, which refers to the mean distance at which velocity vectors are oriented in the same direction, was further extracted as a quantitative parameter of cell movement coordination. α-cat KD cells exhibited low coordinated motion with a correlation length of 50 μm as opposed to values around 150–200 μm for wt MDCK cells, as reported by Vedula *et al.* (2012). Correlation lengths were comparable for α-cat-Δmod and α-cat-wt cells. However, the correlation length was significantly lower for α-cat-L344P cells than for α-cat-wt cells, denoting an altered coordinated behavior as in the case of α-catenin knockdown (Figure 4D). Collective epithelial cell movements are thus strongly dependent on the ability of α-catenin to bind vinculin.

An increased stability of cell–cell contacts, by limiting neighbor exchange within the monolayer as reported in the context of epithelial monolayer aging (Garcia *et al.*, 2015), may directly explain a more coordinated cell behavior and vice versa. This was confirmed by quantifying the effect of the vinculin-binding capability of α-catenin on the lifetime of cell–cell contacts in monolayers coexpressing RFP-Ftractin (Figure 4E and Supplemental Videos 5–8). Although the cell–cell contact lifetime was less than 1 h for α-cat KD cells, it was 4.7 ± 2.6 h for α-cat-L344P cells and increased to 7.7 ± 3.4 h and 12.6 ± 6.1 h for α-cat-wt and α-cat-Δmod cells, demonstrating that the binding of vinculin to α-catenin is required for maintaining stable cell–cell contacts during collective motion of epithelial cells. To support further that the α-catenin/vinculin interaction is responsible for cell–cell contact stability, we analyzed cell–cell contact lifetime in vinculin KD MDCK monolayers (Sumida *et al.*, 2011). Vinculin KD MDCK cells had very short cell–cell contact lifetimes with a mean value of 2.7 ± 1.7 h in between the one measured for α-cat KD cells and the one measured for α-cat L344P cells. However, due to the strong effect of vinculin knockdown on cell–substratum adhesion, it was not possible to draw conclusions about the effect on the correlation length and velocity of the monolayer movement. Thus, we show here that coordinated motion of epithelial cells is dependent on the ability of α-catenin to bind vinculin, which drastically increases cell–cell contact lifetime and correlated movements.

Altogether our results show that the force-dependent interaction between α-catenin and vinculin is crucial for epithelial cells to develop stable but adaptive cell–cell contacts in response to the mechanical resistance of their environment as well as for long-range cell–cell interactions and tissue-scale mechanics. The fact that the association between the two proteins, manipulated here by mutagenesis and mechanical control, has a direct incidence on collective cell movements put the core α-catenin and vinculin mechanosensing machinery at the center of the control of morphogenetic processes.

MATERIALS AND METHODS

Cell culture

MDCK (from the American Type Culture Collection), MDCK αE-catenin knockdown (Benjamin *et al.*, 2010), and MDCK vinculin knockdown (Sumida *et al.*, 2011) cells were maintained in DMEM/Glutamax 10% fetal bovine serum (FBS) and 100 μg/ml penicillin/streptomycin at 37°C in 5% CO_2. Cells were electroporated using an Amaxa system (Nucleofector Device; Lonza) under the following conditions 24 h before experiments: 1×10^6 cells, kit L, and 5 μg of DNA.

Expression vectors

The wt GFP-α-catenin expression vector coding for GFP fused in the N-terminal of mouse αE-catenin was described previously (Thomas *et al.*, 2013). L344P GFP-α-catenin wt mCherry-α-catenin was derived from the wt construct by PCR and DNA ligation. Δmod GFP-α-catenin was obtained by deleting the sequence coding for residues 509–628 (domains MII and MIII according to Desai *et al.*, 2013).

Immunofluorescence staining

Cells were fixed for 15 min with phosphate buffer saline (PBS), 4% formaldehyde, permeabilized with 0.15% Triton X-100 in PBS for 5 min, then incubated with primary antibodies (anti-vinculin mouse monoclonal antibody [1/200, clone 7F9; Millipore], rabbit polyclonal anti-α-catenin and anti-β-catenin [1/400; Sigma], and rat α18 monoclonal anti-αE-catenin antibody [1/200; A. Nagafuchi, Kumamoto University]) in PBS, 1.5% bovine serum albumin (BSA) for 2 h at room temperature. The secondary antibodies (Jackson Laboratories) and Alexa-643 phalloidin (Molecular Probes) were incubated for 1 h in PBS–BSA.

Polyacrylamide substrates

The preparation of PAA was adapted from Pelham and Wang (1997). The PAA gel formulations were prepared from a solution of 2%

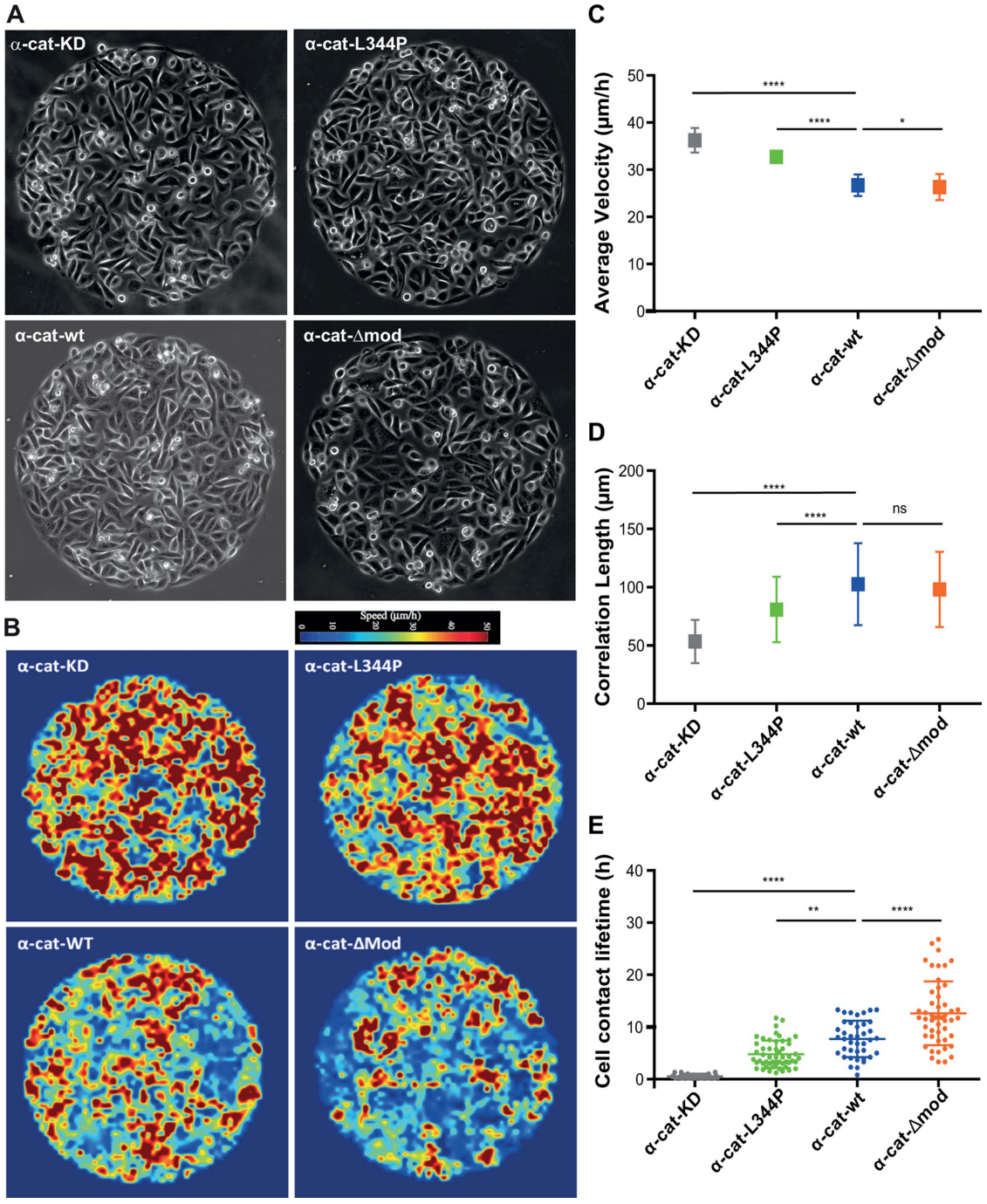

FIGURE 4: Vinculin/α-catenin association controls collective cell behavior and cell–cell contact lifetime. (A) MDCK cells silenced for α-catenin (α-cat KD), as well as cells expressing α-cat-L334P, α-cat-Δmod, or wt α-catenin (α-cat-wt), were seeded on 500-μm Ø FN patterns and phase contrast imaged for 24–36 h (still images of Supplemental Videos 1–4). The collective behavior of cell monolayers was analyzed by PIV over 6 h providing heat maps of instantaneous local velocities (B). Mean velocities (C) and correlation lengths (D) characteristic of each cell type were then extracted from these instantaneous velocity maps (mean values ± SD) out of three independent experiments; $n = 360$ frames analyzed per condition, derived from 10 patterns per condition coming from three independent experiments. ****, $p < 0.0001$; *, $p < 0.1$; ns, nonsignificant; one-way ANOVA test. (E) Mean lifetime of individual cell–cell contacts measured for each cell type (scatter dot plot: mean ± SD, $n = 30$ cell doublets for α-cat KD and α-cat-wt, and $n = 51$ for α-cat-L334P, α-cat-Δmod, out of ≥4 patterns derived from ≥2 independent experiments for each condition; ****, $p < 0.0001$; **, $p < 0.01$; one-way ANOVA test).

bis-acrylamide and 40% acrylamide (Bio-RAD) in 10 mM HEPES. bis-Acrylamide and acrylamide were first combined and allowed to rest for 15 min. Next, 1/1000 total volume TEMED (Bio-RAD) and 1/100 total volume 10% ammonium persulfate (Bio-RAD) were added to the PAA solution together with 2 mg/ml *N*-hydroxysuccinimide (NHS)-ester (Sigma) to allow the formation of covalent bonds

between PAA and FN so that FN remains attached to the PAA gel after removal of the stamped coverslip. The concentrations of acrylamide and bis-acrylamide were adjusted to obtain Young's moduli of 4.5, 9, and 35 kPa, according to Tse and Engler (2010).

Micropatterning

PDMS (poly-dimethylsiloxane) stamps were molded and cured as described previously (Vedula *et al.*, 2014) on silicon wafers (IEMN [Lille, France] or MBI [NUS, Singapore]). A thin layer of PDMS was spin coated over a 35-mm plastic Petri dish and cured at 80°C for 2 h and then exposed to UV for 15 min in a UVO cleaner (Jelight Company). PDMS stamps were incubated with a solution of FN/Cy3-conjugated FN (10/1 ratio, 50 μg/ml; Millipore) for 45 min, washed with water and air dried, then gently pressed against the surface to transfer FN. Regions outside the patterns were blocked with 0.2% Pluronics F-127 (Sigma) for 1 h and washed three times with PBS.

Alternatively, PAA substrates were patterned. For this, air-dried FN-coated PDMS stamps were brought into contact with a cleaned 22 × 22 mm glass coverslip. A second cleaned coverslip, serving as the base for the gel, was silanized by dipping in an ethanol solution containing 2% (vol/vol) 3-(trimethoxysilyl) propyl methacrylate silane (Sigma) and 1% (vol/vol) acetic acid for 5 min. A PAA solution (20 μl) was placed between the silanized coverslip and the FN-stamped one. After 45 min of polymerization the patterned coverslip was removed and the coverslip with the gel, on which patterned FN had been transferred, was placed in a solution of 10 mM HEPES.

Videomicroscopy

Transfected cells were seeded at subconfluency on 500 μm Ø FN patterns in DMEM, 10% fetal calf serum, allowed to attach for 4 h, washed with culture medium, then live imaged (phase contrast and fluorescence) at low magnification (10× BioStation; Nikon) every 10 min for 36 h. The monolayer behavior was analyzed from the time cells entirely occupy the patterns by PIV performed on phase contrast images, to obtain instantaneous velocity fields and correlation length in motion within the cellular disks (Strale *et al.*, 2015).

Fluorescence image acquisition and analysis

Preparations were imaged either with a wide-field fluorescence microscope (Olympus IX81) equipped with a 60× oil immersion objective and a Coolsnap HQ CCD camera, or with a Leica Sp5-II confocal microscope with a 63× oil immersion objective with a distance of 0.5 μm between each plane in the z-stacks. Protein recruitments at cell–cell contacts were determined on z-stack confocal images encompassing the apical cell domain of the monolayer (three most apical stacks) analyzed by the "surfaces" module of Imaris software, applying background subtraction, thresholding of junction area, and removal of objects outside the junctions. Then the mean intensities of the different stainings were measured in the volume of junctions.

Fluorescence recovery after photobleaching

Fluorescence recoveries after photobleaching were performed at 37°C, 24 h posttransfection, using the Leica Sp5-II setup. Argon laser power was set at 50%. Acousto-optic tunable filter (AOTF) output power was set at 10% for pre- and postbleach acquisition and at 100% for bleaching. Fluorescence was acquired for 6.5 s at a frequency of 0.8 s^{-1}, over a whole field, then a Ø 2-μm region of interest (ROI) was bleached for 3 s, followed by acquisition over the whole field for 26 s at a frequency of 0.8 s^{-1}, then for 300 additional seconds at a frequency of 0.1 s^{-1}. After correction for photobleaching, the normalized recovery of fluorescence was expressed as a ratio of prebleach fluorescence, as reported previously (Lambert *et al.*, 2007). Fluorescence recoveries in function of time were fitted with one-term exponential equations, allowing one to extract a plateau value representing the fraction of diffusion-limited molecules (mobile fraction) and a recovery half-time ($t_{1/2}$) proportional to the apparent diffusion coefficient of diffusion-limited molecules (Thoumine *et al.*, 2006). The mobile fraction and the $t_{1/2}$ were determined by fitting the normalized recovery curves using the one-phase decay nonlinear regression function of the GraphPad Prism 5.01 software.

Magnetic tweezers cytometry

Ecad-Fc–coated bead doublets attached to the surface of transfected cells were submitted to magnetic twisting using an in-house–built magnetic tweezers. Bead doublets were used instead of individual beads to increase the applied torque and facilitate subsequent image analysis. The bead doublets were made by mixing antibody immobilized Ecad-Fc–coated beads with protein A–coated beads; therefore, only one bead of the doublet binds to the cell through E-cadherin interaction. Bead doublet rotation was captured while the rotation of the magnet was simultaneously recorded. The fluctuation angle of the bead doublet relative to its original direction was calculated to obtain its response to magnet rotation, and the SD of the fluctuation angle was extracted. More specifically, protein A–coated paramagnetic beads (2.8 μm from Dynabeads) were washed three times and incubated overnight at room temperature with anti-human Fc fragment antibody in 0.1 M borate buffer, pH 8. After three washes, the beads were resuspended in Ca^{++} and Mg^{++} containing PBS and incubated for 3 h at room temperature with recombinant Ecad-Fc (R&D Systems). These Ecad-Fc–coated beads were mixed with equal amounts of uncoated protein A beads and incubated for 1 h at room temperature to form bead doublets. The bead solution was then resuspended in PBS, 1% BSA, sonicated, and incubated for 20–30 min at 37°C, 5% CO_2 with adherent transfected cells. GFP-positive cells displaying a bead doublet were selected for the magnetic twisting experiment. The torque was applied thanks to a homemade magnetic twisting cytometer (360° in clockwise and anticlockwise directions at a constant speed of 5°/s). Bead displacement was captured with an inverted microscope equipped with a 50× long working distance objective lens and a camera (Pike from Allied Vision) with 100 Hz sampling frequency while the rotation of the magnet was recorded directly. The image sequence of the bead doublets was loaded into ImageJ. The image stack was thresholded to only highlight the contours of the bead doublet, and other features of the image—like cell contours—were removed manually. The "Directionality" plug-in of the Fiji package was used to calculate the principle orientations of the bead doublet. The fluctuation angle of the bead was matched to the direction of the magnet to obtain its response to magnet rotation. The SD of the fluctuation angle was used as a measure of the bead–cell interaction stiffness. For a bead that follows the magnet directly, denoting a very soft interaction between the bead and the cell cortex, the SD is around 60°; for very strong mechanical coupling between the bead and the cortex, this value is close to 0°.

PIV analysis

PIV analysis of monolayer movement was performed as described in Petitjean *et al.* (2010) using the MatPIV v. 1.6.1 package and implemented in MATLAB MatPIV—the PIV toolbox for MATLAB—available at http://folk.uio.no/jks/matpiv/Download/index2.html. Cross-correlation techniques were performed to compute the displacement vectors at each subwindow by finding their best match at the successive time frame. The analysis was done with 32 × 32 pixel

(19 × 19 μm) interrogation windows with an overlap of 50%. The correlation length was then calculated using the formula previously described (Petitjean *et al.*, 2010). Velocity values obtained were the mean of the norm of all velocity vectors extracted from each image. For this study, we consider the mean velocities over a time interval of 6 h to minimize the effects of cell division, time zero being the moment at which cells reach confluency.

Lifetime of cell–cell contacts

The appearance and disappearance of individual cell–cell contacts were tracked over time on time-laps of RFP-Ftractin fluorescence movies. The *t* zero was set when two cells initiate a contact and the separation time is the time at which the two cells separated within the monolayer.

Statistical analysis and curve fitting and image processing

Statistical analysis and curve fitting were performed with GraphPad Prism 5.0 software. Image processing was done in ImageJ (or MATLAB when indicated), then with Photoshop and Illustrator.

ACKNOWLEDGMENTS

This work was supported by grants from the Centre National de la Recherche Scientifique (CNRS), Université Paris-Diderot (R.M.M., B.L.), NUS-SPC (National University of Singapore-Université Sorbonne-Paris-Cité), and Projet International de Coopération Scientifique (PICS) CNRS programmes (R.M.M.), Fondation ARC pour la recherche sur le cancer (R.M.M.), the Human Frontier Science Program (Grant no. RPG0040/2012; B.L. and R.M.M.), the LABEX "Who am I?," and Agence Nationale de la Recherche (ANR 2010 Blan1515). B.L. is supported by the European Research Council under the European Union's Seventh Framework Programme (FP7/2007–2013/ERC [European Research Council] Grant agreement no. 617233) and the Mechanobiology Institute. R.S. has been supported by a C'nano program Région Ile de France doctoral fellowship and Fondation pour la Recherche Médicale (FRM) (FDT20140930851). We acknowledge the IJM ImagoSeine Imaging Facility, member of the France BioImaging infrastructure supported by the French National Research Agency (ANR-10-INSB-04, "Investments of the future").

REFERENCES

Bazellieres E, Conte V, Elosegui-Artola A, Serra-Picamal X, Bintanel-Morcillo M, Roca-Cusachs P, Munoz JJ, Sales-Pardo M, Guimera R, Trepat X (2015). Control of cell–cell forces and collective cell dynamics by the intercellular adhesome. Nat Cell Biol 17, 409–420.

Benjamin JM, Kwiatkowski AV, Yang C, Korobova F, Pokutta S, Svitkina T, Weis WI, Nelson WJ (2010). αE-catenin regulates actin dynamics independently of cadherin-mediated cell–cell adhesion. J Cell Biol 189, 339–352.

Buckley CD, Tan J, Anderson KL, Hanein D, Volkmann N, Weis WI, Nelson WJ, Dunn AR (2014). Cell adhesion. The minimal cadherin-catenin complex binds to actin filaments under force. Science 346, 1254211.

Chen CS, Hong S, Indra I, Sergeeva AP, Troyanovsky RB, Shapiro L, Honig B, Troyanovsky SM (2015). α-Catenin–mediated cadherin clustering couples cadherin and actin dynamics. J Cell Biol 210, 647–661.

Collins C, Nelson WJ (2015). Running with neighbors: coordinating cell migration and cell–cell adhesion. Curr Opin Cell Biol 36, 62–70.

Desai R, Sarpal R, Ishiyama N, Pellikka M, Ikura M, Tepass U (2013). Monomeric α-catenin links cadherin to the actin cytoskeleton. Nat Cell Biol 15, 261–273.

Doxzen K, Vedula SR, Leong MC, Hirata H, Gov NS, Kabla AJ, Ladoux B, Lim CT (2013). Guidance of collective cell migration by substrate geometry. Integr Biol (Camb) 5, 1026–1035.

Dufour S, Mege RM, Thiery JP (2013). α-Catenin, vinculin, and F-actin in strengthening E-cadherin cell–cell adhesions and mechanosensing. Cell Adhes Migr 7, 345–350.

Garcia S, Hannezo E, Elgeti J, Joanny JF, Silberzan P, Gov NS (2015). Physics of active jamming during collective cellular motion in a monolayer. Proc Natl Acad Sci USA 112, 15314–15319.

Guillot C, Lecuit T (2013). Mechanics of epithelial tissue homeostasis and morphogenesis. Science 340, 1185–1189.

Han MK, Hoijman E, Noel E, Garric L, Bakkers J, de Rooij J (2016). αE-Catenin-dependent mechanotransduction is essential for proper convergent extension in zebrafish. Biol Open 5, 1461–1472.

Hansen SD, Kwiatkowski AV, Ouyang CY, Liu H, Pokutta S, Watkins SC, Volkmann N, Hanein D, Weis WI, Mullins RD, Nelson WJ (2013). αE-Catenin actin-binding domain alters actin filament conformation and regulates binding of nucleation and disassembly factors. Mol Biol Cell 24, 3710–3720.

Hoffman BD, Yap AS (2015). Towards a dynamic understanding of cadherin-based mechanobiology. Trends Cell Biol 25, 803–814.

Huveneers S, de Rooij J (2013). Mechanosensitive systems at the cadherin–F-actin interface. J Cell Sci 126(Pt 2), 403–413.

Jurado J, de Navascues J, Gorfinkiel N (2016). α-Catenin stabilises Cadherin-Catenin complexes and modulates actomyosin dynamics to allow pulsatile apical contraction. J Cell Sci 129, 4496–4508.

Kim TJ, Zheng S, Sun J, Muhamed I, Wu J, Lei L, Kong X, Leckband DE, Wang Y (2015). Dynamic visualization of α-catenin reveals rapid, reversible conformation switching between tension states. Curr Biol 25, 218–224.

Kobielak A, Fuchs E (2004). α-Catenin: at the junction of intercellular adhesion and actin dynamics. Nat Rev Mol Cell Biol 5, 614–625.

Ladoux B, Nelson WJ, Yan J, Mege RM (2015). The mechanotransduction machinery at work at adherens junctions. Integr Biol (Camb) 10, 1109–1119.

Lambert M, Thoumine O, Brevier J, Choquet D, Riveline D, Mege RM (2007). Nucleation and growth of cadherin adhesions. Exp Cell Res 313, 4025–4040.

le Duc Q, Shi Q, Blonk I, Sonnenberg A, Wang N, Leckband D, de Rooij J (2010). Vinculin potentiates E-cadherin mechanosensing and is recruited to actin-anchored sites within adherens junctions in a myosin II-dependent manner. J Cell Biol 189, 1107–1115.

Leckband D, Prakasam A (2006). Mechanism and dynamics of cadherin adhesion. Annu Rev Biomed Eng 8, 259–287.

Lien WH, Klezovitch O, Fernandez TE, Delrow J, Vasioukhin V (2006). αE-catenin controls cerebral cortical size by regulating the hedgehog signaling pathway. Science 311, 1609–1612.

Maki K, Han SW, Hirano Y, Yonemura S, Hakoshima T, Adachi T (2016). Mechano-adaptive sensory mechanism of α-catenin under tension. Sci Rep 6, 24878.

Mayor R, Etienne-Manneville S (2016). The front and rear of collective cell migration. Nat Rev Mol Cell Biol 17, 97–109.

Mege RM, Ishiyama N (2017). Integration of cadherin adhesion and cytoskeleton at adherens junctions. Cold Spring Harb Perspect Biol 9, a028738.

Pelham RJ Jr, Wang YI (1997). Cell locomotion and focal adhesions are regulated by substrate flexibility. Proc Natl Acad Sci USA 94, 13661–13665.

Peng X, Cuff LE, Lawton CD, DeMali KA (2010). Vinculin regulates cell-surface E-cadherin expression by binding to β-catenin. J Cell Sci 123, 567–577.

Peng X, Maiers JL, Choudhury D, Craig SW, DeMali KA (2012). α-Catenin uses a novel mechanism to activate vinculin. J Biol Chem 287, 7728–7737.

Petitjean L, Reffay M, Grasland-Mongrain E, Poujade M, Ladoux B, Buguin A, Silberzan P (2010). Velocity fields in a collectively migrating epithelium. Biophys J 98, 1790–1800.

Ray S, Foote HP, Lechler T (2013). β-Catenin protects the epidermis from mechanical stresses. J Cell Biol 202, 45–52.

Silvis MR, Kreger BT, Lien WH, Klezovitch O, Rudakova GM, Camargo FD, Lantz DM, Seykora JT, Vasioukhin V (2011). α-Catenin is a tumor suppressor that controls cell accumulation by regulating the localization and activity of the transcriptional coactivator Yap1. Sci Signal 4, ra33.

Strale PO, Duchesne L, Peyret G, Montel L, Nguyen T, Png E, Tampe R, Troyanovsky S, Henon S, Ladoux B, Mege RM (2015). The formation of ordered nanoclusters controls cadherin anchoring to actin and cell–cell contact fluidity. J Cell Biol 210, 333–346.

Sumida K, Igarashi Y, Toritsuka N, Matsushita T, Abe-Tomizawa K, Aoki M, Urushidani T, Yamada H, Ohno Y (2011). Effects of DMSO on gene expression in human and rat hepatocytes. Hum Exp Toxicol 30, 1701–1709.

Takeichi M (2014). Dynamic contacts: rearranging adherens junctions to drive epithelial remodelling. Nat Rev Mol Cell Biol 15, 397–410.

Thomas WA, Boscher C, Chu YS, Cuvelier D, Martinez-Rico C, Seddiki R, Heysch J, Ladoux B, Thiery JP, Mege RM, Dufour S (2013). α-Catenin and vinculin cooperate to promote high E-cadherin–based adhesion strength. J Biol Chem 288, 4957–4969.

Thoumine O, Lambert M, Mege RM, Choquet D (2006). Regulation of N-cadherin dynamics at neuronal contacts by ligand binding and cytoskeletal coupling. Mol Biol Cell 17, 862–875.

Torres M, Stoykova A, Huber O, Chowdhury K, Bonaldo P, Mansouri A, Butz S, Kemler R, Gruss P (1997). An α-E-catenin gene trap mutation defines its function in preimplantation development. Proc Natl Acad Sci USA 94, 901–906.

Tse JR, Engler AJ (2010). Preparation of hydrogel substrates with tunable mechanical properties. Curr Protoc Cell Biol, Chapter 10, Unit 10.16.

Vasioukhin V, Bauer C, Degenstein L, Wise B, Fuchs E (2001). Hyperproliferation and defects in epithelial polarity upon conditional ablation of α-catenin in skin. Cell 104, 605–617.

Vedula SR, Leong MC, Lai TL, Hersen P, Kabla AJ, Lim CT, Ladoux B (2012). Emerging modes of collective cell migration induced by geometrical constraints. Proc Natl Acad Sci USA 109, 12974–12979.

Vedula SRK, Ravasio A, Anon E, Chen T, Peyret G, Ashraf M, Ladoux B (2014). Microfabricated environments to study collective cell behaviors. Methods Cell Biol 120, 235–252.

Vermeulen SJ, Bruyneel EA, Bracke ME, De Bruyne GK, Vennekens KM, Vleminckx KL, Berx GJ, van Roy FM, Mareel MM (1995). Transition from the noninvasive to the invasive phenotype and loss of α-catenin in human colon cancer cells. Cancer Res 55, 4722–4728.

Yao M, Qiu W, Liu R, Efremov AK, Cong P, Seddiki R, Payre M, Lim CT, Ladoux B, Mege RM, Yan J (2014). Force-dependent conformational switch of α-catenin controls vinculin binding. Nat Commun 5, 4525.

Yonemura S, Wada Y, Watanabe T, Nagafuchi A, Shibata M (2010). α-Catenin as a tension transducer that induces adherens junction development. Nat Cell Biol 12, 533–542.